Research article

SURFACE and INTERFACE ANALYSIS

Received: 17 October 2011 Revised: 23 February 2012 Accepted: 27 March 2012 Published online in Wiley Online Library: 11 May 2012

(wileyonlinelibrary.com) DOI 10.1002/sia.5019

Nanotribological behavior of thermal treatment of zinc titanate thin films

Shyh-Chi Wu,[a,b] Wei-Hung Yau,[c] Chien-Huang Tsai[d]* and Chang-Pin Chou[a]

We present a study of the nanotribological behavior of $ZnTiO_3$ films; the surface morphology, stoichiometry, and friction (μ) were analyzed using atomic force microscopy, X-ray photoelectron spectroscopy, and nanoscratch system. It is confirmed that the measured values of H and μ of the $ZnTiO_3$ films were in the range from 8.5 ± 0.4 to 5.6 ± 0.4 GPa and from 0.164 to 0.226, respectively. It is suggested that the hexagonal $ZnTiO_3$ decomposes into cubic Zn_2TiO_4 and rutile TiO_2 based on the thermal treatment; the H, μ, and R_{MS} were changed owing to the grain growth and recovery that results in a relax crystallinity of $ZnTiO_3$ films. From X-ray photoelectron spectroscopy measured, core levels of O 1 can attribute the weaker bonds as well as lower resistance after thermal treatment. The XRD patterns showed that as-deposited films are mainly amorphous; however, the hexagonal $ZnTiO_3$ phase was observed with the $ZnTiO_3$ (104), (110), (116), and (214) peaks from 620 to 820 °C, indicating that there is highly (104)-oriented $ZnTiO_3$ on the silicon substrate. Copyright © 2012 John Wiley & Sons, Ltd.

Keywords: radio frequency magnetron co-sputtering; friction; atomic force microscopy; X-ray photoelectron spectroscopy

Introduction

TiO_2 and ZnO[1–11] have attracted wide attention; they serve a promising strategy for degradation of pollutant in the role of photocatalytic semiconductors. Henceforth, TiO_2 has high recombination rate of the photo-induced surface electron–hole pairs. ZnO has a low quantum yield in the photocatalytic reactions.[12,13] Recently, there has been growing interest in the novel material of zinc oxide and titanium dioxide composite. $ZnTiO_3$ composite form was conducted as the promising materials due to its good semiconducting, dielectric properties,[14–16] and etc.,[17–22] which leads to wide applications in sensors, microelectronics, and high-performance catalysts.[23–27] Notice that most studies are limited to the analyses of phase, composition, and microstructure of the film; three compounds, as-Zn_2TiO_4 (cubic), $ZnTiO_3$ (hexagonal), and $Zn_2Ti_3O_8$ (cubic), existing in the ZnO–TiO_2 system have been reported.[23] It was also found that $ZnTiO_3$ film is zinc metatitanate with a hexagonal structure and titanium dioxide, while the film of Zn/Ti ratio is lower than 1. Nanometer-scale nanoindentation is often employed to provide controllable crack information relating to the mechanical characteristics of the solid surfaces, including the hardness (H) and Young's modulus (E).[28,29] These properties must be enhanced through the basic improvement of the intrinsic properties of the $ZnTiO_3$ film through the composition or the extrinsic properties including structure, grain size, morphology, etc. H and residual stress are important parameters for tribological coatings.[30,31] Obayashi *et al*. regarded the three compounds of $ZnTiO_3$ film;[23] however, their studies still can be thoroughly studies by nanoindentation technique, such as phase formation of thin film with different annealing temperatures. The quality responsible for the system of $ZnTiO_3$ film therefore becomes an interesting issue in terms of the effect on the resulting tribological characteristics.

In the present study, pure $ZnTiO_3$ films were prepared by RF magnetron co-sputtering process; the effect of thermal treatment of $ZnTiO_3$ films was reported. We employed nanoscratch techniques to investigate the response of the $ZnTiO_3$ film; their adhesion and/or cohesion failure relative to chemical bonding was analyzed by scanning probe microscopy/atomic force microscopy and X-ray photoelectron spectroscopy.

Experimental details

The $ZnTiO_3$ films were prepared by RF magnetron co-sputtering system using 4-in-diameter sintered ceramic target of ZnO and TiO_2 (>99.9%). In the co-sputtering, the sputtering rate of ZnO is higher than TiO_2. We follow the early report[32] that the $ZnTiO_3$ film with Zn/Ti atomic ratio of 1:1 is achieved while their area ratio of ZnO to TiO_2 is about 1:26 in the sputtering conditions. In order to obtain stoichiometric deposit $ZnTiO_3$ films on Si substrate, Ar-O_2 flow (8:2) with a purity of 99.999 gas of 50 sccm was introduced into the chamber with mass flow controllers, and RF powers at 200 W were used. In addition, the sputtering pressure was 2×10^{-2}, the substrate temperature was set at 250 °C, and the duration of the deposition was 1 h. To remove the contaminants formed on the target surface and to stabilize the sputtering conditions, it was necessary for pre-sputtering to be

* *Correspondence to: Chien-Huang Tsai, Automation Engineering, Nan Kai University of Technology, Nantou 54243, Taiwan, ROC. E-mail: chtsai12@gmail.com*

a *Department of Mechanical Engineering, National Chiao Tung University, Hsinchu 300, Taiwan, ROC*

b *Chung Shan Institute of Science and Technology (CSIST), Taoyuan 325, Taiwan, ROC*

c *Department of Mechanical Engineering, Chin-Yi University of Technology, Taichung 400, Taiwan, ROC*

d *Department of Automation Engineering, Nan Kai University of Technology, Nantou 54243, Taiwan, ROC*

SURFACE and INTERFACE ANALYSIS

performed for 5 min prior to each deposition process. The detailed deposition conditions of the $ZnTiO_3$ films are listed in Table 1. Those specimens were subsequently subjected to *ex situ* thermal treatment in a furnace under N_2 gas for 2 h with a heating rate of 5 °C/min at 520, 620, 720, and 820 °C, respectively. The pure inert gas N_2 (>99.999%) is selected that can avoid the impurity element from air environment.

After deposition, the surface roughness and adhesion are analyzed by scanning probe microscopy/atomic force microscopy (SPM/AFM, Triboscipe, Hystron, MN) that have been used to perform the nanoscratch tests for these samples with a constant scan speed of $2\mu ms^{-1}$. The average surface roughness R_{ms} of the current sample is recorded. In addition, the H values of the $ZnTiO_3$ films were determined using a Nano Indenter XP instrument (MTS Cooperation, Nano Instruments Innovation Center, TN, USA). Chemical bonding states and chemical compositions of the films were analyzed by X-ray photoelectron spectroscopy (XPS, VG Scientific Microlab 310F). Inductively coupled plasma-mass spectrometer was applied to determine the element concentrations in the films, which confirmed that the stoichiometry of $ZnTiO_3$ films. Crystallinity of the films was analyzed by X-ray diffraction (PANalytical X'Pert Pro (MRD), with Cu Kα (λ = 0.154 nm) radiation for 2θ from 20° to 80° at a scan speed of $2°min^{-1}$, and a grazing angle of 0.5° under 30 kV and 30 mA.

Results and discussion

In Fig. 1 are shown the XRD patterns of the $ZnTiO_3$ films, (a) as-deposited, and the annealing treatment was (b) 520, (c) 620, (d) 720, and (e) 820 °C. It was observed that there were no diffraction peaks in the XRD pattern for as-deposited films [Fig. 1(a)]. It is suggested that the film structure is mainly amorphous. The main hexagonal $ZnTiO_3$ phase (104) is firstly displayed from the annealing treatment sample which was 520 °C [Fig. 1 (b)]. Herein, as the annealing treatment sample was 620 °C, the hexagonal $ZnTiO_3$ phase was observed with the $ZnTiO_3$ (104), (110), (116), and (214) peaks, respectively [Fig. 1 (c)]. The intensities of the (104) peak were higher than the other peaks of $ZnTiO_3$ films at 820 °C [Fig. 1 (c)–1(e)], indicating that there is highly (104)-oriented $ZnTiO_3$ on the silicon substrate. From the recently reported,[33] the preferred orientation tends to reduce its free energy to reach a stable state; this is the same case in our experimental data. The $ZnTiO_3$ structure is also comparable with the XPS that Zn–O and Ti–O binding energy at 533 and 536 eV is strong as the annealing treatment sample was 620 °C. However, the low Zn–O and Ti–O binding energy is displayed due to more

Table 1. RF sputter conditions for the zinc titanate films

Target	$ZnTiO_3$
Target size in diameter (in.)	4
Target to substrate distance (mm)	90
RF power (W)	200
Chamber pressure (Torr)	$5x10^{-6}$
Working pressure (Torr)	$2x10^{-2}$
Sputtering gas	Ar
Ar-O_2 folw (sccm)	50 (8:2)
Substrate temperature (°C)	250
Deposition time (min)	120

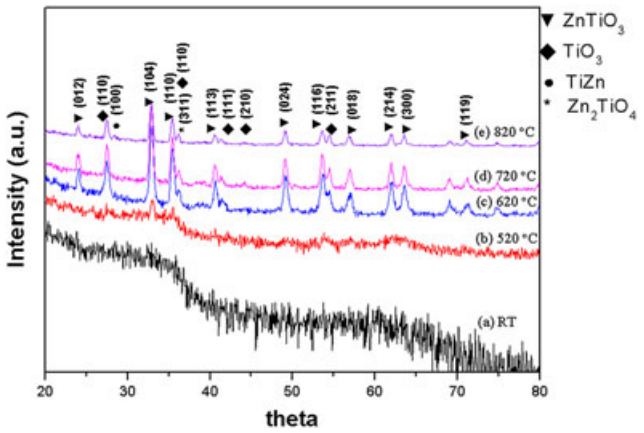

Figure 1. X-ray diffraction patterns of the $ZnTiO_3$ films (a) as-deposited at RT, and different thermal temperatures (b) 520, (c) 620, (d) 720, and (e) 820 °C.

chemical impurity from XPS analysis; thus, the ZnTi (110) structure has a weak diffraction peaks in the XRD pattern at 820 °C. We attributed that the hexagonal $ZnTiO_3$ decomposed into cubic Zn_2TiO_4 and TiO_2 (rutile) from 620 to 820 °C, the $ZnTiO_3$ phase remained stable at a temperature of 820 °C.[34]

Figure 2 shows AFM inspections of $ZnTiO_3$ films deposited with silicon substrate as well as the subsequent nanoscratch measured. First, small cavities and bright particles can be directly observed from the thermal condition at RT to 620 °C; this trend was observed that the cavities are due to the evaporation of Zn, and the white particles are TiO_2.[35–37] One can easily know good distribution of grain sizes from 720 to 820 °C which is denser than that of RT. We suggest that a high thermal temperature enhances the atomic mobility and causes the grain recovery. We can find that the surface roughness is increased from 3, 3, 3.9, and 5.8 to 20.6 nm while the thermal temperature increased from RT to 820 °C. It is shown that the surface morphologies of the samples became rough and grains grew at thermal environment.[38–40] There are five typical AFM profiles and the lateral forces were a ramped load of 1000 μN for all of the samples [Fig. 2(a)–2(e)]. In this perspective, we point out that the features of the nanoscratch zone in the vicinity of the interface may not be just accidental artifacts resulting from sample preparation. In Table 2, we presented the increase in the values of R_{MS}, while the annealing treatment sample was from 520 to 820 °C. The nanoscratch track corresponding to $ZnTiO_3$ films was observed in the surface profile. The large grain boundary was observed at the condition of 820 °C instead of RT. Therefore, in order to investigate the trend of grain boundary distribution of $ZnTiO_3$ films, we display typical friction coefficients plotted with respect to the scratch duration for each sample (Fig. 3). One can observe the onset of the marked oscillations under the friction force and abrupt oscillations in both the on-load and off-load scans at the condition of 520 °C instead of RT. The increase in the thermal temperature over 620 °C features more sudden oscillating fluctuations than those from RT to 520 °C. We inspect that the lower degrees of adhesion reflect interlinks, and rearrangements tend to result in fluctuations of the values of μ. The uncertainty of initial μ profile, namely pile-up, occurred in some of the samples at high thermal treatment; it is associated with the settling down of the indenter head, particularly in the low-load region. The values of μ of the $ZnTiO_3$ films with respect to the thermal temperature were determined by averaging those measured at scratch durations ranging from 8 to 40 s (Fig. 3).

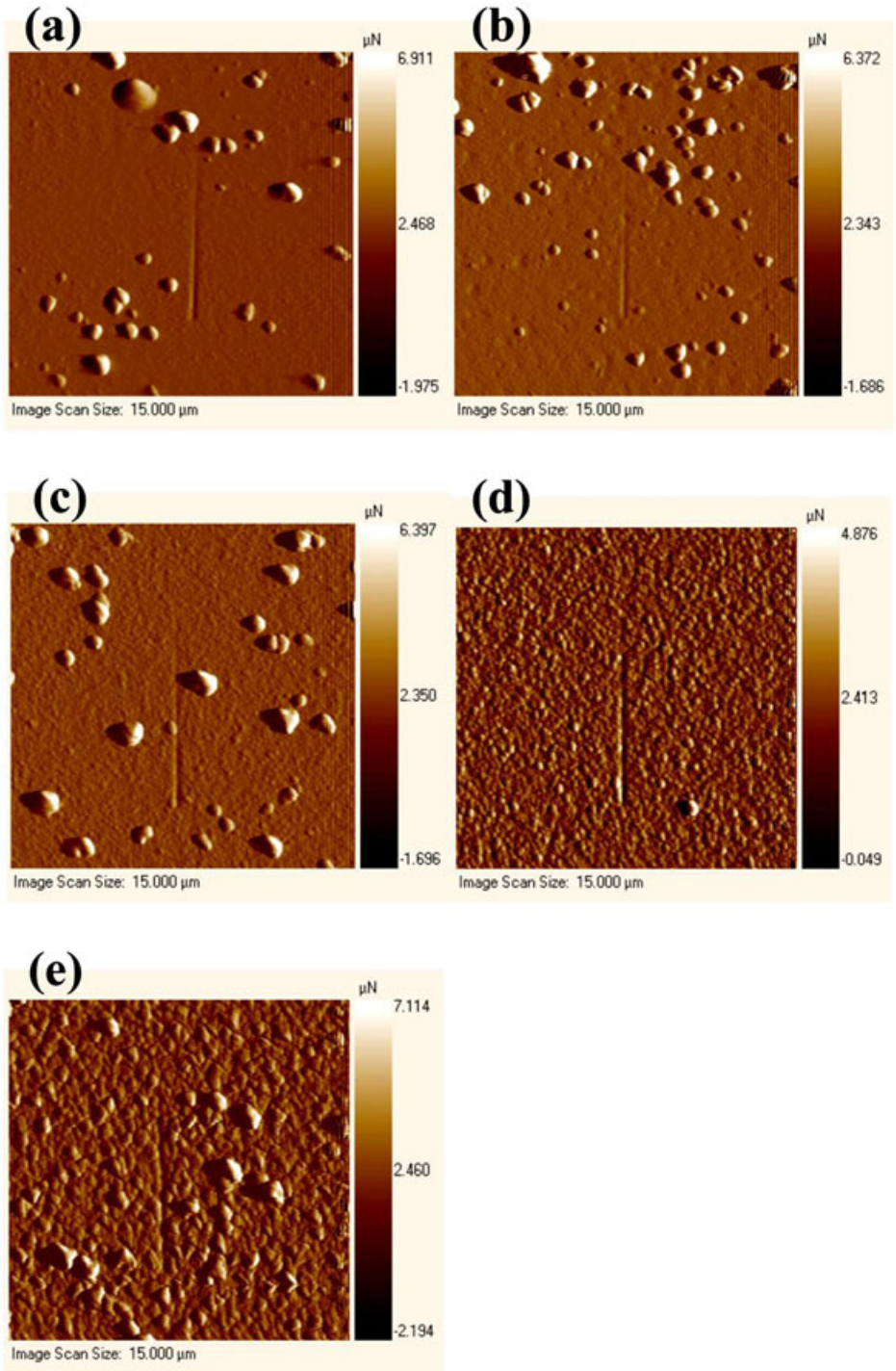

Figure 2. 3D-AFM images of the surfaces of $ZnTiO_3$ films and the features of the nanoscratch traces zone: (a) RT, (b) 520, (c) 620, (d) 720, and (e) 820 °C.

Table 2. The summaries of $ZnTiO_3$ film with respect to the H, R_{MS}, μ, and later force

$ZnTiO_3$	Hardness (GPa)	R_{MS} (n m)	Friction	Lateral Force (μ N)
As-deposited	8.5 ± 0.4	3	0.164	60.3
620°C	11.4 ± 0.4	3	0.186	53.6
620°C	10.5 ± 0.4	3.9	0.197	64.7
720°C	9.6 ± 0.5	5.8	0.208	68.7
820°C	5.6 ± 0.4	20.6	0.226	77.6

The obtained discordant curves and irregularities appeared in the course of plastic deformation due to the continuity adhesion and/or cohesion failure; those transitions were determined from the nanoscratch traces and pile up. The profile, however, at the condition of 820 °C is softer than that of RT due to the shrinking of nanoscratch traces. It is indicated that the structure of $ZnTiO_3$ films is changed with thermal atmosphere from 520 to 820 °C, which induces the variation of the composition in the intrinsic structure. Hence, the bulge edge scenarios can be connected between the groove and film, and then the material was crushed

SURFACE and INTERFACE ANALYSIS

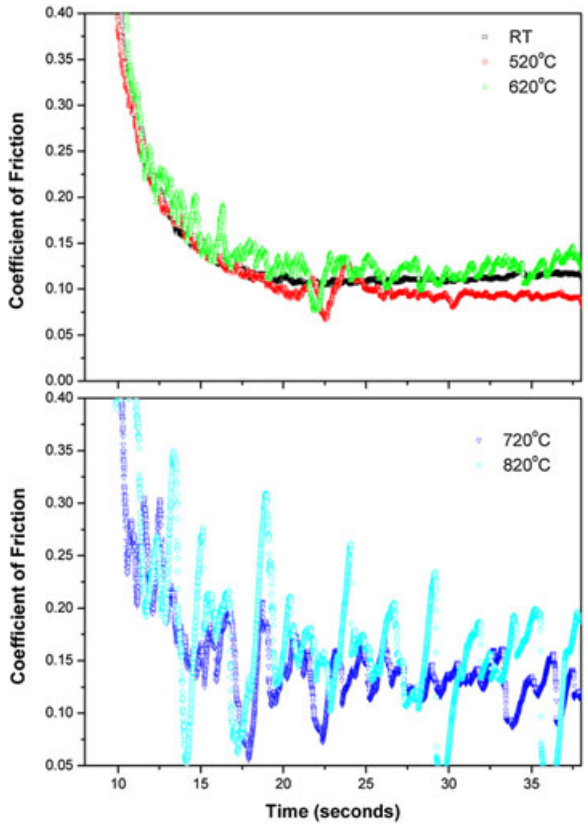

Figure 3. Five typical profiles of the coefficient of friction (μ) *versus* scratch duration at the variation of thermal condition of the $ZnTiO_3$ films: RT, 520, 620, 720, and 820 °C.

as a result of elastic failure. Notice that the friction traces were fairly reproducible, but exhibited great variability for each sample. In Table 2, we presented increase in the values of μ, lateral force, and R_{MS}, and the decrease in the values of H with increasing annealing temperature. Notably, changes in thermal treatment resulted in different failure events occurring in Fig. 2.

The presented co-sputtering $ZnTiO_3$ film can be achieved with Zn/Ti atomic ratio of 1:1 in Fig. 4; XPS measurement confirmed the as-deposited Ti 2p: 15.6% and Zn $2p^3$: 14.8% and the annealed temperature of 820 °C, Ti 2p: 14% and Zn $2p^3$: 18.1%.

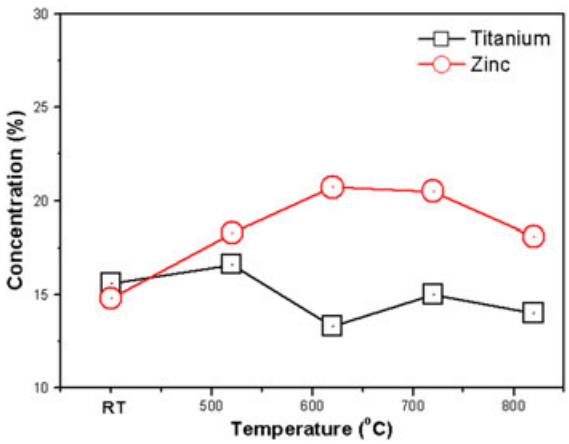

Figure 4. The stoichiometric change of $ZnTiO_3$ thin films treated by conventional annealing condition: RT, 520, 620, 720, and 820 °C.

The constituent elements of the $ZnTiO_3$ films were measured. The chemical compositions (O 1s) of the films deposited at variation of thermal treatment were shown in Fig. 5. The XPS spectra have been charge corrected to the adventitious Ti 2p and Zn $2p^3$. The binding energy of the O 1s states is located from 530 to 538 eV, which depended on the thermal treatment that splits in their peaks under various growth procedures of $ZnTiO_3$ films are clearly examined. It is concluded that a main phase $ZnTiO_3$ into Zn_2TiO_4 and TiO_2 occurred in association with the increase of thermal annealing.[41] Also, other groups conclude that the $ZnTiO_3$ phase decomposed from Zn_2TiO_4 and rutile TiO_2 above 945 °C while increasing the annealing temperature.[42,43] In the presented, one can observe the part of O–Zn bond formation (binding energy at 529.4 eV and 531.5 eV) at the thermal treatment from RT to 520 °C that the peak positions are in good agreement with the Zn–O bond and some Ti–O bond.[44,45] From Lee *et al.*,[39] they report that the films (RT) are amorphous, however, the onset of crystallization occurred at annealing temperatures 600 °C (cubic phase $Zn_2Ti_3O_8$), 700 °C (hexagonal phase; $ZnTiO_3$), and exceeding 900 °C (cubic Zn_2TiO_4 and rutile TiO_2). The crystal texture of $ZnTiO_3$ films can influence their nanotribological properties at different annealing treatment stage; the comparison of phase transformation of $ZnTiO_3$ films was performed by XRD pattern as well. Grain growth and strain energy are processed at the inner film that can often be a dominant factor. From XPS observation, the thermal treatment from 620 to 720 °C is evidence that the main chemical bonding may be coexisting as Zn–O (binding energy at 531.5) and Ti–O (binding energy at 533 and 536 eV). This trend is also studied in detail by Huang *et al.*.[40] The films (RT) are amorphous columnar structure, and further crystallization (500–900 °C) was observed as $ZnTiO_3$ (hexagonal) and TiO_2 (rutile) coexisted. That is to say, in metal oxides, the intrinsic defects such as oxygen vacancies and metal ion interstitials usually coexist. We conclude that the lower H values of the $ZnTiO_3$ film can be induced by some reason, including the packing factor, stoichiometry, residual stress, preferred orientation, and grain size.[44] A low value of R_{ms} is beneficial to a $ZnTiO_3$ film because it can be used to provide information regarding its morphology; the surface morphologies of our films were relatively rough and non-uniformly distributed. In addition, the grain size in the $ZnTiO_3$ film increases obviously with higher thermal treatment, casing many gaps between grain

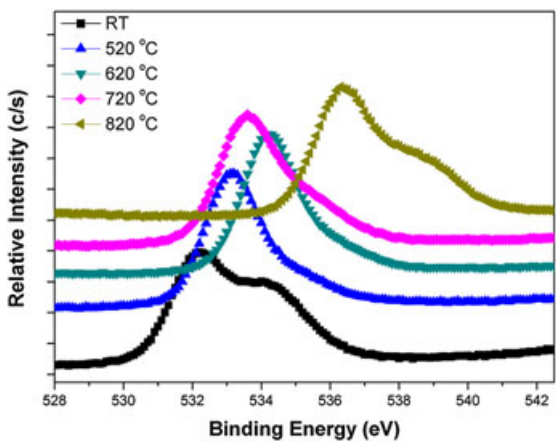

Figure 5. XPS core level spectra (O1s) of $ZnTiO_3$ films on Si substrate with respect to the variation of annealing condition: RT, 520, 620, 720, and 820 °C.

boundaries due to the abnormal grain growth. Nanoscratch result reveals a variation of adhesion and/or cohesion failure transition around the indentation regions of the $ZnTiO_3$ films. The initial deformation, elastic deformation, and residual deformation of the $ZnTiO_3$ films were studied at the thermal treatment.

Conclusion

The XRD patterns of the $ZnTiO_3$ films showed that there were no diffraction peaks in the XRD pattern for as-deposited films because the film structure is mainly amorphous. The hexagonal $ZnTiO_3$ phase was observed with the $ZnTiO_3$ (104), (110), (116), and (214) peaks over 620 °C. The intensities of the (104) peak were higher than the other peaks of $ZnTiO_3$ films at 820 °C, indicating that there is highly (104)-oriented $ZnTiO_3$ on the silicon substrate. The effects of transformation of the co-sputtering $ZnTiO_3$ films were investigated by nanoindenter technique. The measured values of H and μ of the $ZnTiO_3$ films were in the range from 8.5 ± 0.4 to 5.6 ± 0.4 GPa and from 0.164 to 0.226, respectively. Slight oscillations and discontinuous phenomena manifested in each μ profile due to the thermal relaxation in $ZnTiO_3$ films. The XPS core level analysis of the $ZnTiO_3$ films has been measured for O 1s, and the change is due to the Zn–Ti complex compound that alters the H, μ, and R_{MS}. The R_{MS} in the $ZnTiO_3$ film increases relatively with thermal treatment, thus many gaps are observable from AFM between grain boundaries. A variation of adhesion and/or cohesion failure transition around the crack regions of the $ZnTiO_3$ films by means of nanoscratch investigation was observed.

References

[1] S. C. Pillai, P. Periyat, R. George, D. E. McCormack, M. K. Seery, H. Hayden, J. Colreavy, D. Corr, S. J. Hinder, *J. Phys. Chem. C* **2007**, *111*, 1605–1611.
[2] A. Muruganandham, N. Shobana, A. Swaminathan, *J. Mol. Catal. A: Chem.* **2006**, *246*, 154–161.
[3] W. S. Kuo, P. H. Ho, *Dyes Pigments* **2006**, *71*, 212–217.
[4] S. Sakthivel, B. Neppolian, M. V. Shankar, B. Arabindoo, M. Palanichamy, V. Murugesan, *Sol. Energy Mater. Sol. Cells* **2003**, *80*, 65–82.
[5] S. K. Kansal, M. Singh, D. Sud, *J. Hazard. Mater.* **2007**, *141*, 581–590.
[6] E. Evgenidou, K. Fytianos, I. Poulios, *Appl. Catal. B: Environ.* **2005**, *59*, 81–89.
[7] M. Muruganandham, N. Sobana, M. Swaminathan, *J. Hazard. Mater.* **2006**, *137*, 1371–1376.
[8] B. Neppolian, H. C. Choi, S. Sakthivel, B. Arabindoo, V. Murugesan, *J. Hazard. Mater.* **2002**, *89*, 303–317.
[9] S. K. Pardeshi, A. B. Patil, *J. Hazard. Mater.* **2009**, *163*, 403–409.
[10] C. Karunakaran, S. Senthilvelan, S. Karuthapandian, *Sol. Energy Mater. Sol. Cells* **2005**, *89*, 391–402.
[11] K. M. Parida, S. Parija, *Sol. Energy* **2006**, *80*, 1048–1054.
[12] D. Chatterjee, S. Dasgupta, N. N. Rao, *Sol. Energy Mater. Sol. Cells* **2006**, *90*, 1013–1020.
[13] Y. H. Jiang, Y. M. Sun, H. Liu, F. H. Zhu, H. B. Yin, *Dyes Pigments* **2008**, *78*, 77–83.
[14] C. F. Shih, W. M. Li, M. M. Lin, K. T. Hung, *J. Electrochemical Soc.* **2009**, *156*, E13–E17.
[15] H. T. Kim, *Mater. Res. Bull.* **1998**, *33*, 963–973.
[16] A. Golovchansky, H. T. Kim, Y. H. Kim, *J. Kor. Phys. Soc.* **1998**, *32*, 1167–1169.
[17] H. T. Kim, S. Nahm, J. D. Byun, *J. Am. Ceram. Soc.* **1999**, *82*, 3476–3480.
[18] H. Obayashi, Y. Sakurai, T. Gejo, *J. Solid State Chem.* **1976**, *17*, 299–303.
[19] Z. X. Chen, A. Derking, W. Koot, M. P. van Dijk, *J. Catal.* **1996**, *161*, 730–741.
[20] K. H. Yoon, J. Cho, D. H. Kang, *Mater. Res. Bull.* **1999**, *34*, 1451–1461.
[21] E. Hosono, S. Fujihara, M. Onuki, T. Kimura, *J. Am. Ceram. Soc.* **2004**, *87*, 1785–1788.
[22] S. F. Wang, M. K. Lu, F. Gu, C. F. Song, D. Xu, D. R. Yuan, S. W. Liu, G. J. Zhou, Y. X. Qi, *Inorg. Chem. Commun.* **2003**, *6*, 185–188.
[23] H. Obayashi, Y. Sakurai, T. Gejo, *J. Solid. State. Chem.* **1976**, *17*, 299–303.
[24] Z. X. Chen, A. Derking, W. Koot, M. P. van Dijk, *J. Catal.* **1996**, *161*, 730–741.
[25] K. H. Yoon, J. Cho, D. H. Kang, *Mater. Res. Bull.* **1999**, *34*, 1451–1461.
[26] E. Hosono, S. Fujihara, M. Onuki, T. Kimura, *J. Am. Ceram. Soc.* **2004**, *87*, 1785–1788.
[27] F. H. Dulin, D. E. Rase, *J. Am. Ceram. Soc.* **1960**, *43*, 125–131.
[28] Y. M. Chang, H. C. Wen, C. S. Yang, D. Lian, C. H. Tsai, J. S. Wang, W. F. Wu, C. P. Chou, *Microelectron. Reliab.* **2010**, *50*, 1111–1115
[29] H. C. Wen, C. S. Yang, W. C. Chou, *Appl. Surf. Sci.* **2010**, *256*, 2128–2131.
[30] M. H. Lin, H. C. Wen, Y. R. Jeng, C. P. Chou, *Nanoscale Res. Lett.* **2010**, *5*(11), 1812–1816
[31] M. H. Lin, H. C. Wen, Z. C. Chang, S. C. Wu, W. F. Wu, C.-P. Cho, *Surface and Interface Anal.* **2010**, *43*, 918–9221.
[32] C. Ye, Y. Wang, Y. Ye, J. Zhang, G. H. Li, *J. Appl. Phys.* **2009**, *106*, 033520–4.
[33] Y. C. Lee, Y. L. Huang, W. H. Lee, F. S. Shieu, *Thin Solid Films* **2010**, *518*, 7366–7371.
[34] M. Sugiura, K. Ikeda, *J. Jpn. Ceram. Assoc.* **1947**, *55*, 62–66.
[35] Y. S. Chang, Y. H. Chang, I. G. Chen, G. J. Chen, Y. L. Chai, *J. Cryst. Growth* **2002**, *243*, 319–326.
[36] G. A. Hutchins, G. H. Maher, S. D. Ross, Am. *Ceram. Soc. Bull.* **1987**, *66*(4), 681–684.
[37] Y. S. Chang, Y. H. Chang, I. G. Chen, G. J. Chen, Y. L. Chai, *J. Cryst. Growth.* **2002**, *243*, 319–326.
[38] M. C. Chiu, Y. C. Lee, F. S. Shieu, *J. Electronchemical Soc.* **2005**, *150*, F194–F199.
[39] Y. C. Lee, Y. L. Huang, W. H. Lee, F. S. Shieu, *Thin Solid Films* **2010**, *518*, 7366–7371.
[40] Y. L. Huang, Y. C. Lee, D. C. Tsai, F. S. Shieu, *Mater. Sci. Forum.* **2011**, *687*, 610–613.
[41] J. S. Jung, Y. H. Kim, S. K. Gil, D. H. Kang, *J Electroceram* **2009**, *23*, 272–276.
[42] F. H. Dulin, D. E. Rase, *J. Am. Ceram. Soc.* **1960**, *43*, 125–131.
[43] O. Yamaguchi, M. Morimi, H. Kawabata, K. Shimizu, *J. Am. Ceram. Soc.* **1987**, *70*, 97–98.
[44] B. R. Strohmeier, D. M. Hercules, *J. Catal.* **1984**, *86*, 266.
[45] Md. N. Islam, T. B. Ghosh, K. L. Chopra, H. N. Acharya, *Thin Solid Films* **1996**, *280*, 211–220.